Journal of Power Sources 265 (2014) 239–245

Contents lists available at ScienceDirect

Journal of Power Sources

journal homepage: www.elsevier.com/locate/jpowsour

Ultrathin carbon nanopainting of $LiFePO_4$ by oxidative surface polymerization of dopamine

Bo Ding [a], Wei Chin Tang [b], Ge Ji [b], Yue Ma [a], Pengfei Xiao [c], Li Lu [c], Jim Yang Lee [a,*]

[a] NUS Graduate School for Integrative Sciences and Engineering (NGS), Center for Life Sciences (CeLS), #05-01 28 Medical Drive, Singapore 117456, Singapore
[b] Department of Chemical and Biomolecular Engineering, National University of Singapore, 10 Kent Ridge Crescent, Singapore 119260, Singapore
[c] Department of Mechanical Engineering, National University of Singapore, 9 Engineering Drive 1, Singapore 117576, Singapore

HIGHLIGHTS

- A facile coating method based on redox chemistry of Fe^{3+} and dopamine.
- Ultrathin, and uniform carbon coating of $LiFePO_4$.
- Excellent electrochemical performance for reversible Li^+ storage (143 mAh g^{-1} at current density of 1700 mA g^{-1}).

GRAPHICAL ABSTRACT

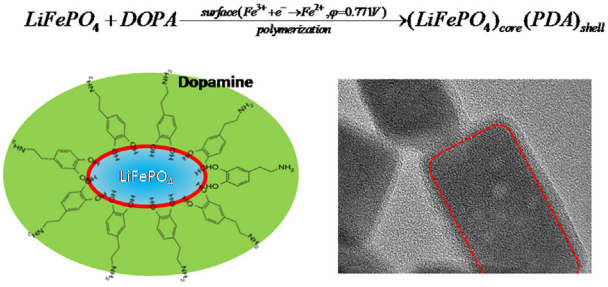

ARTICLE INFO

Article history:
Received 8 March 2014
Received in revised form
21 April 2014
Accepted 25 April 2014
Available online 6 May 2014

Keywords:
Surface polymerization
Dopamine
Carbon coating
Phosphate cathode
Lithium ion battery

ABSTRACT

The common strategy to address the low electronic conductivity of $LiFePO_4$ is to downsize $LiFePO_4$ and to coat the nanocrystal with conductive carbon film. The major issues with existing carbon coating techniques are thickness and quality control. This paper reports a facile carbon coating method which can provide ultrathin, uniform and fully encapsulating carbon coating on $LiFePO_4$. This coating method capitalizes on the redox chemistry of surface Fe^{3+} on solvothermally synthesized $LiFePO_4$ nanocrystal, to deposit uniform thin films of polydopamine films. The polymer film is easily carbonized into ultrathin carbon film. The carbon coated $LiFePO_4$ exhibits very high rate performance (143 mAh g^{-1} at current density of 1700 mA g^{-1}) with excellent capacity retention.

1. Introduction

Cost, safety and environmental considerations have determined that conventional $LiCoO_2$-based lithium ion batteries are not quite suitable for large-scale applications such as electric vehicles and grid energy storage. Such considerations are better met by olivine structured phosphates $LiMPO_4$ (where M = Fe, Mn, Co and Ni) [1–7]. Among the phospho-olivines $LiFePO_4$ has the longest history of research and is hence the most developed. $LiFePO_4$ has a flat voltage plateau at 3.4 V *vs* Li^+/Li and a high theoretical specific capacity of 170 mAh g^{-1}. [1] Although the attainable specific energy density of $LiFePO_4$ is only marginally higher than that of $LiCoO_2$, $LiFePO_4$ provides exceptional safety, nontoxicity, and cycle stability. The major deficiency of $LiFePO_4$ is the low intrinsic electronic and ionic conductivities common to all phospho-olivines, which severely limit its performance in power-oriented applications [2,3].

* Corresponding author. Tel.: +65 6516 2899; fax: +65 67791936.
E-mail address: cheleejy@nus.edu.sg (J.Y. Lee).

http://dx.doi.org/10.1016/j.jpowsour.2014.04.131
0378-7753/

Two strategies are commonly used to improve the power performance of $LiFePO_4$. One is to downsize crystalline $LiFePO_4$ to the nanoscale for shorter electron and Li^+ diffusion lengths and consequently faster transport in the solid state [7–9]. The other is to modify the nanocrystal surface with an electron conductor, commonly a carbon film, to reduce the external electrical resistance [1,2,10–16]. These two strategies are commonly used in tandem to maximize performance [17,18]. Most carbon coatings derived from a carbonaceous precursor lack good uniformity. The conductivity of the carbon coating can be improved by graphitization at high temperature. The heat treatment, however, introduces the side effect of increasing crystallite size. The two strategies can therefore be mutually compensating resulting in the trade-off between crystal size reduction and carbon conductivity increase [10,19,20]. Therefore, the development of a low temperature method which can fully and uniformly encapsulate the $LiFePO_4$ nanocrystals with a high conductivity coating is of great practical significance. The coating thickness should be as thin as possible to reduce the resistance to Li^+ diffusion through the coating.

This report presents here a facile coating method which can produce an ultrathin, uniform and fully encapsulating carbon coating on $LiFePO_4$ nanocrystals. The coating method capitalizes on the redox chemistry of Fe^{3+}, which are present on the surface of solvothermally synthesized $LiFePO_4$ nanocrystals, to deposit a uniform thin film of carbon precursor by the oxidative polymerization of an aromatic amine. The oxidizing Fe^{3+} is formed by the low temperature solvothermal synthesis to compensate for the lithium deficiency in $LiFePO_4$ nanocrystals [21,22]. There is also accumulation of Fe^{3+} in the surface region due to the ease of Fe^{2+} oxidation when $LiFePO_4$ is exposed to atmospheric O_2 [23,24]. Dopamine (DOPA), a naturally occurring compound with catechol and amine moieties which confer it with extremely strong adhesive properties, was selected as the aromatic monomer [25–30]. Dopamine has been used as a carbon source for lithium ion battery anode materials before [31,32]. The procedure involves the base-catalysed polymerization of dopamine with an external oxidizer followed by product separation and waste disposal. Reaction conditions have to be carefully controlled to achieve uniform deposition of the polymerized film. By comparison the surface polymerization reported here is simple, spontaneous, and without the need for external oxidizers or separation. The in-situ generated polymer film on the crystallite surface is also highly uniform in thickness and surface coverage. Scheme 1 shows that the presence of Fe^{3+} on the $LiFePO_4$ nanocrystal surface is central to this simple and yet effective carbon coating method, which uses the high oxidation power of Fe^{3+} ($\varphi(Fe^{3+/2+}) = 0.771$ V *vs.* SHE [33]) to bring about the *in-situ* polymerization of adsorbed DOPA to polydopamine (PDA) on the $LiFePO_4$ nanocrystals. The catechol groups bound strongly to the $LiFePO_4$ surface to form a uniform, strongly adherent and fully encapsulating thin DOPA film. There was no need for extraneous chemicals such as base buffer and oxidizer. The PDA layer on the nanocrystal surface was then pyrolysed at high temperature into a carbon film. $LiFePO_4$ recrystallization was suppressed by the carbon encapsulation to retain the nanoscale advantage of $LiFePO_4$. It is worth noting that the plenitude of phenyl rings in PDA is conducive to the formation of highly graphitized sp^2 domains by calcination. The presence of nitrogen atoms in the carbon film could further increase the film conductivity [34,35]. Most importantly the oxidative surface also provided film thickness control since thickness could not grow beyond a monolayer coverage due to the self-limiting nature of the polymerization process. Consequently the coating was ultra-thin (1–2 nm thick) amounting to around 1 wt.% of carbon in the $LiFePO_4$/C composite. The carbon content is lower than all previously reported $LiFePO_4$/C composites [18,36–38]. Since carbon in the cathode is electrochemically inactive and its low density can decrease the overall volumetric energy density, a low carbon content in the $LiFePO_4$/C composite is a desired material specification. Consequently the synthesized core–shell $LiFePO_4$/C nanocomposite displayed excellent power capability, delivering 84% (143 mAh g^{-1}) of the theoretical capacity even at a high 10 C rate ($C = 170$ mA g^{-1}). This coating method is therefore effective for increasing the performance of $LiFePO_4$.

2. Experimental section

2.1. Synthesis of $LiFePO_4$ nanoparticles

LFP nanoparticles were synthesized by the solvothermal method published by Nan et al. with some modifications. [21] 27 mmol $LiOH \cdot H_2O$ was first dissolved in 20 ml ethylene glycol. A mixture of 10 mmol H_3PO_4 and 5 ml ethylene glycol was introduced drop-wise to the LiOH solution with stirring. A white colloid was formed from the neutralization reaction. A solution containing 10 mmol $FeSO_4 \cdot 7H_2O$ in 15 ml ethylene glycol was then added to the colloid in a drop-wise manner. A dark green colloid was formed and was allowed to stir for 1 h. The mixture was transferred to a Teflon-lined autoclave and heated at 180 °C for 10 h. Upon cooling to room temperature, the solid product was recovered by centrifugation and washed successively with ethanol and water thrice in the centrifuge.

2.2. In-situ DOPA polymerization

111.57 mg dopamine hydrochloride (~10 wt.% of synthesized $LiFePO_4$) was added to a 50 ml dispersion of the $LiFePO_4$ nanocrystals in H_2O. The mixture was ultrasonicated for 1 h. The dark purple $LiFePO_4$/PDA precipitate was removed from the solution by vacuum filtration and allowed to dry in an 80 °C oven for 2 h. The dried $LiFePO_4$/PDA composite was then calcined at 650 °C for 3 h in Ar to form $LiFePO_4$/C.

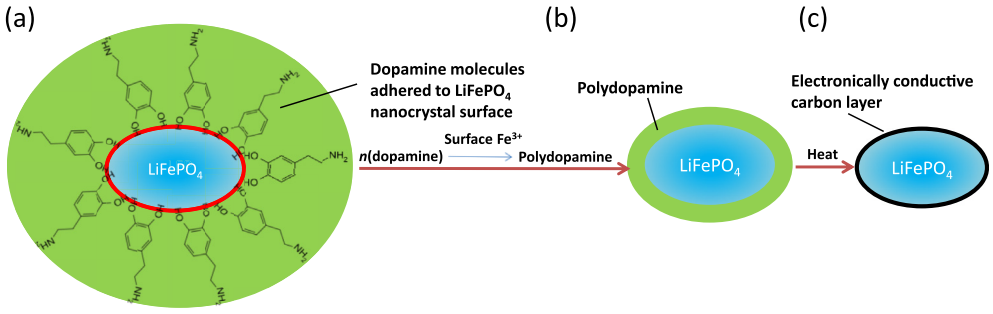

Scheme 1. Schematic illustrations of: (a) adsorbed dopamine molecules on $LiFePO_4$ nanocrystal surface; (b) in-situ polymerization of dopamine by surface Fe^{3+} ions into a polydopamine shell on $LiFePO_4$ nanocrystal; (c) the thin carbon shell on $LiFePO_4$ nanocrystal.

2.3. Materials characterization

The phase purity of $LiFePO_4$/C was determined by XRD on a Bruker D8 advance X-ray diffractometer with Cu Kα radiation (1.5405 Å). Morphology examinations were based on field emission scanning electron microscopy (FESEM) (on a JEOL JSM-6700F) and field emission transmission electron microscopy (FETEM) (on a JEOL 2100F). The carbon content in $LiFePO_4$/C was determined by thermal gravimetric analysis (TGA) in the temperature range 20 °C–800 °C on a Shimadzu DTG-60H. X-ray photoelectron spectroscopy (XPS) was performed on a VG ESCALAB MKII spectrometer operating at 25 kV. Binding energies were corrected using 284.0 eV for the C1s peak as reference. A JASCO FTIR-Q250 spectrometer was used to record the infrared absorption spectrum of $LiFePO_4$/C in the 4000–400 cm^{-1} spectral region (2 cm^{-1} resolution and 50 scans). The KBr pellet method (1 wt.% sample and 99 wt.% KBr) was used for IR sample preparation.

2.4. Electrochemical measurements

An electrode slurry was prepared by mixing $LiFePO_4$/C, poly(-vinylidene fluoride) (PVdF) and Super-P in a 8:1:1 weight ratio in *N*-methylpyrrolidone (NMP) and stirring vigorously for 16 h. The resultant slurry was applied to an Al foil to an areal density of ~3 mg cm^{-2}. The counter and reference electrode was a lithium metal foil and the separator was a Celgard 2400 membrane. The electrolyte was a 1 M $LiPF_6$ in a mixture of ethylene carbonate (EC), dimethyl carbonate (DMC) and diethyl carbonate (DEC) (1:1:1 vol./vol.). The electrodes were assembled into a Swagelok cell in an Ar-filled glove box. Galvanostatic charging and discharging of the batteries was carried out on a Neware BTS-5V-10 mA battery tester, and cyclic voltammetry was performed on a μAutolab type III electrochemical workstation.

3. Results and discussion

The $LiFePO_4$ in this study was prepared by solvothermal synthesis. In the preparation $LiOH\cdot H_2O$, H_3PO_4 and $FeSO_4\cdot 7H_2O$ were dissolved separately in ethylene glycol. The mixing of $LiOH\cdot H_2O$ and H_3PO_4 formed a colloidal Li_3PO_4 solution which could more effectively control the precipitation of $Fe_3(PO_4)_2\cdot xH_2O$ in the next sequence of $FeSO_4\cdot 7H_2O$ solution addition. Due to the solubility difference between Li_3PO_4 ($K_{sp} = 3.2 \times 10^{-9}$) and $Fe_3(PO_4)_2\cdot xH_2O$ ($K_{sp} = 1 \times 10^{-32}$), this particular sequence of solution mixing avoided the fast precipitation of $Fe_3(PO_4)_2\cdot xH_2O$ by regulating the release of PO_4^{3-} from Li_3PO_4; and suppressed excessive crystal growth and agglomeration. The precipitation of $Fe_3(PO_4)_2\cdot xH_2O$ was allowed to complete in 1 h with stirring, which also introduced some Fe^{2+} oxidation. The $Fe_3(PO_4)_2\cdot xH_2O$ formed as such provided the nucleation sites for the crystal growth of $LiFePO_4$ under solvothermal conditions.

Fig. 1 shows that the solvothermally synthesized $LiFePO_4$ nanocrystals had a plate-like morphology and about 30 nm in thickness. The higher viscosity of ethylene glycol, as compared with solvents such as water or ethanol, could slow the diffusion of ionic reactants in solution and consequently restrained crystal growth. [21] The small plate-like nanocrystals had a large exposed surface where oxidation could occur in air. The XPS spectrum in Fig. 1c shows the Fe oxidation states on the nanocrystal surface. The relative high intensity of the Fe^{3+} signal indicates that the $LiFePO_4$ nanocrystal surface was enriched with Fe^{3+}. The Fe^{3+}-rich surface could then provide the oxidizing power needed to initiate DOPA polymerization. Consequently the adsorption of DOPA ($\varphi \approx 0.2$ V *vs.* SHE) [39] was immediately followed by the polymerization of DOPA on the $LiFePO_4$ surface:

$$LiFePO_4 + DOPA \xrightarrow[\text{polymerization}]{\text{surface}\left(Fe^{3+}+e^- \rightarrow Fe^{2+},\ \varphi = 0.771\ V\right)} (LiFePO_4)_{core}(PDA)_{shell}$$

Some of the surface Fe^{3+} was simultaneously reduced to Fe^{2+}, and the Li^+ which were de-intercalated from $LiFePO_4$ during exposure to air were re-intercalated for charge balance. According to the generally accepted mechanism of oxidative polymerization of DOPA, the catechol group in DOPA was first oxidized to quinone and then polymerization occurred [25,28]. The extent of DOPA polymerization on the surface was therefore controlled by the amount of Li^+ available for charge balance. The amount of Li^+ that can be de-intercalated by oxidation in air has been determined by Martin et al. to be 2.3 mol% using a $LiFePO_4$/C sample synthesized by the solid-state reaction. [24] Since the nanocrystals here were smaller than those in the Martin study, the amount of de-intercalated Li^+ should be larger than 2.3 mol%. Since DOPA was used in excess during the synthesis, all de-intercalated Li^+ were expected to be completely re-intercalated. The TGA results in Fig. 2 indicates that 3.2 mol % of DOPA was polymerized on the $LiFePO_4$ nanocrystal surface, corresponding to 6.4 mol% of de-intercalated Li^+. For the polymerization reaction the $LiFePO_4$ nanocrystals were dispersed well in water before the addition of DOPA. The $LiFePO_4$ colloid was stabilized by the small nanocrystal size and the hydrophilic character of the $LiFePO_4$ surface. There were visual cues of immediate polymerization right after the addition of DOPA to the $LiFePO_4$ colloid – an instantaneous change of the colloid color from dark green to purple; and the progressive darkening of the colloidal solution color with time indicative of the increasing extent of polymerization.

The presence of a PDA shell was confirmed by Fourier transform infrared spectroscopy (FTIR). A typical FTIR spectrum of the $LiFePO_4$/PDA composite is shown in Fig. 3a, where the absorption peaks at 3400 cm^{-1} and 1640–1480 cm^{-1} correspond well with the characteristics of the catechol –OH groups and the phenyl rings of the PDA shell respectively [5,40,41]. The strong absorption from 1200 to 800 cm^{-1} was due to the PO_4^{3-} groups of $LiFePO_4$ [42]. The low intensities of the absorption peaks associated with PDA compared with $LiFePO_4$ indicate that the PDA loading in the composite was low. The thin PDA shell was clearly visible in the TEM images (Fig. 3b–d). The coating layer was very thin and uniform on each nanocrystal. The coating thickness as determined from Fig. 3c and d varied from 2 to 3 nm. This thin PDA shell was later converted to an ultrathin carbon shell after the high temperature treatment.

The XRD pattern in Fig. 4a of $LiFePO_4$/C after heat treatment at 650 °C shows only the diffraction peaks of $LiFePO_4$, indicating high phase purity of the product. The rod-like nanocrystals had an average diameter of 30–50 nm and an average length of 60–100 nm. The SEM and TEM images in Fig. 3b and c indicate that despite the high temperature treatment, the nanocrystals were still well separated without aggregation or coalescence. This could be

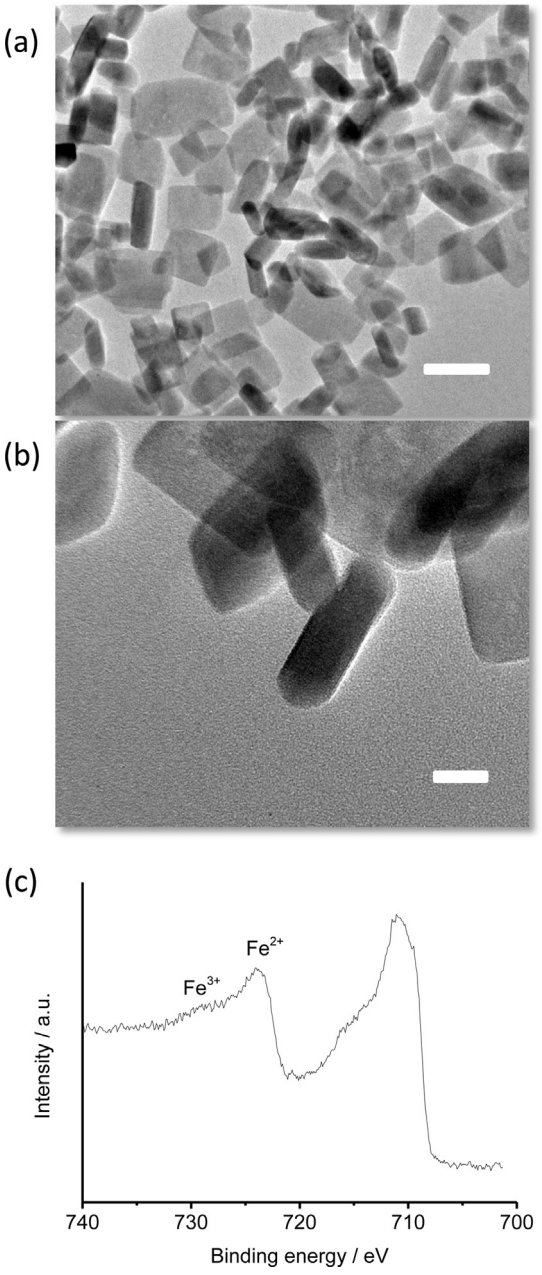

Fig. 1. Characterizations of the solvothermally synthesized $LiFePO_4$ nanocrystals: (a) TEM and (b) HRTEM images (c) XPS spectrum. Scale bars: (a) 50 nm; (b) 30 nm.

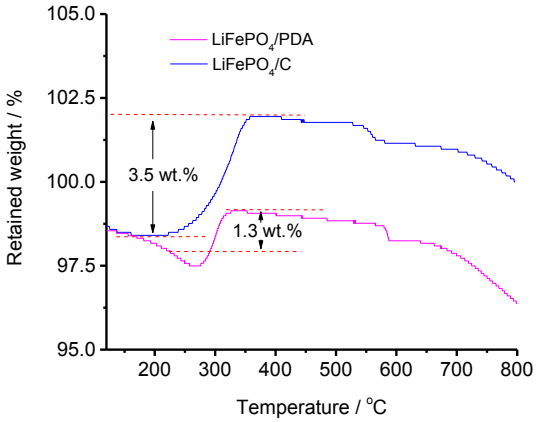

Fig. 2. TGA curves of $LiFePO_4$/PDA and $LiFePO_4$/C. Bare $LiFePO_4$ will gain 5 wt.% upon heating to 200–500, thus a bare 8–10% lithium deficient $Li_{1-x}FePO_4$ would gain around 4.5 wt.% upon heating. Therefore the estimated carbon amount in $LiFePO_4$/C is around 1 wt.%. The estimated PDA amount in $LiFePO_4$/C is around 3.2 wt.%. The loss of weights of both $LiFePO_4$/PDA and $LiFePO_4$/C are suspected to be caused by the decomposition of lithium deficient $Li_{1-x}FePO_4$.

credited to the presence of the uniform carbon surface coating, which inhibited nanocrystal sintering. Not only was the nanoscale advantage of the Li^+ storage host preserved, the electrical integration of the nanocrystals with one another and with the conductivity agent was also made more effective through the encapsulating carbon coating. This can significantly reduce the electron transport resistance between particles to support high-power applications. Fig. 4d and e shows that the carbon shell was uniform all over the nanocrystal surface, with a shell thickness as thin as 1–2 nm. This uniform carbon layer ensured that all $LiFePO_4$ nanocrystals were surface conductive, while the thinness of the thickness assured minimum resistance to the diffusion of Li^+ across the coating. The nitrogen atoms from PDA were also incorporated in the carbon layer to reap the benefits of carbon nitrogenation which could lead to further conductivity increases (See Fig. 5). The nitrogen content in the carbon coating incorporated as such was ~7.4 wt% and it contained both pyrrolic and pyridinic nitrogen. The quality of carbon was measured by Raman spectroscopy (Fig. 6). The resulting I_d/I_g ratio was 0.7, suggesting a good high degree of graphitization. The amount of carbon in $LiFePO_4$/C composite as determined by thermal gravimetric analysis (See Fig. 2) was only 1 wt.%. Since the carbon in the $LiFePO_4$/C composite is electrochemically inactive, the minimization of carbon content can contribute to a higher overall specific energy density of the composite.

However, despite the reduction of Fe^{3+} to Fe^{2+} at the $LiFePO_4$ nanocrystal surface by DOPA polymerization, a significant amount of Fe^{3+} was still present, as shown by the Fe XPS spectrum in Fig. 7. This result also suggests that only a small amount of surface Fe^{3+} was consumed in DOPA polymerization. The presence of surface Fe^{3+} in $LiFePO_4$ indicates that there was a substantial amount of lithium vacancy in the nanocrystals. This inference was verified by the measurement of the columbic efficiency (CE) of the first charge and discharge cycle. The columbic efficiency, which is the ratio of Li^+ inserted into $FePO_4$ (in the discharge process) to the Li^+ extracted from $LiFePO_4$ (in the charge process), was higher than 100% in the first cycle. This was only possible with an as-prepared Li^+-deficient host material. The first cycle CE in Fig. 8 suggests that there were about 8–14 mol% of lithium deficiencies in the $LiFePO_4$ nanocrystals.

The electrochemical performance of $LiFePO_4$/C was evaluated in half cells using lithium metal as the counter cum reference electrode. Fig. 9 shows the cyclic voltammograms (CV) in the 2.5–4.5 V potential range for the first five cycles at 0.1 mV s^{-1}. The two redox peaks at 3.2 V and 3.6 V correspond well with Li^+ intercalation/de-intercalation reactions coupled with the Fe^{2+}/Fe^{3+} redox. Good symmetry between the oxidation and reduction peaks was observed as well as close to unity peak current ratio and low peak potential separation. Collectively these are indications of the good reversibility of the Li^+ intercalation/de-intercalation reactions. It should be noted that the first cycle voltammograms was substantially different from the other 4 cycles. The first cycle oxidation exhibited an asymmetric peak, probably caused by the concentration difference between the Fe^{3+} on the nanocrystal surface and Fe^{3+} in the nanocrystal bulk. The CV features stabilized after the first 5 cycles. Such behaviour is typical of "electrode conditioning" which may be attributed to various activation effects [43,44]. The

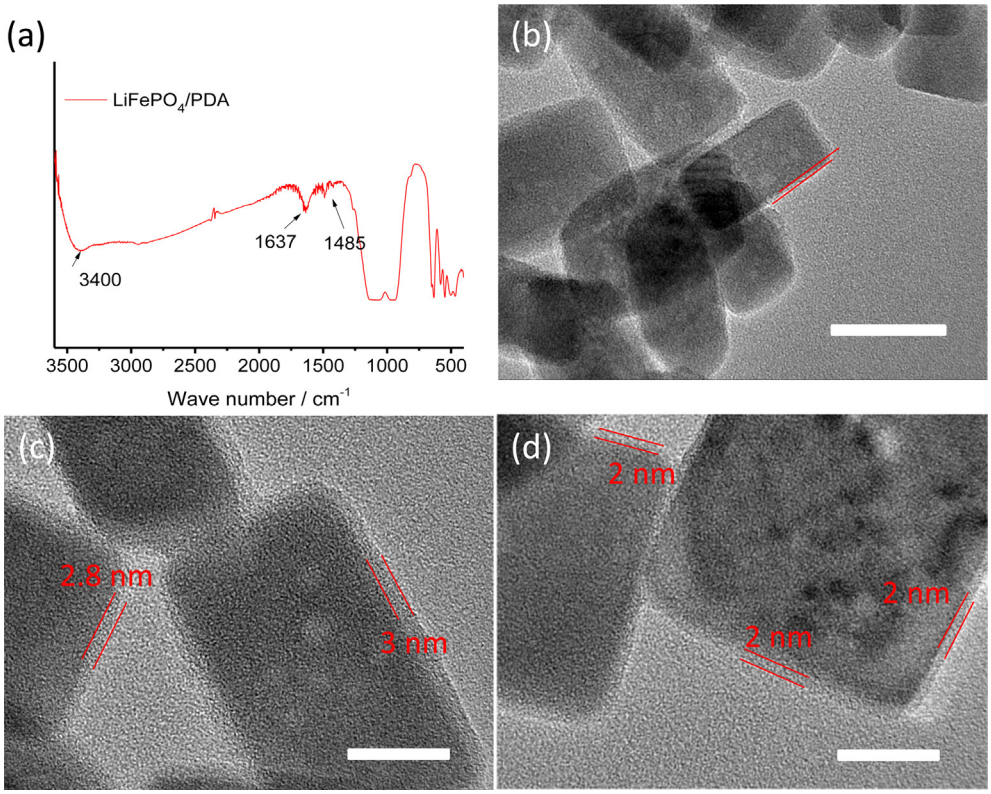

Fig. 3. Characterizations of PDA-coated $LiFePO_4$: (a) FTIR spectrum; (b) TEM image; (c) and (d) HRTEM images. The PDA shell was uniformly coated on the nanocrystal surface to a shell thickness of 2–3 nm. Scale bars: (b) 50 nm; (c) and (d) 20 nm.

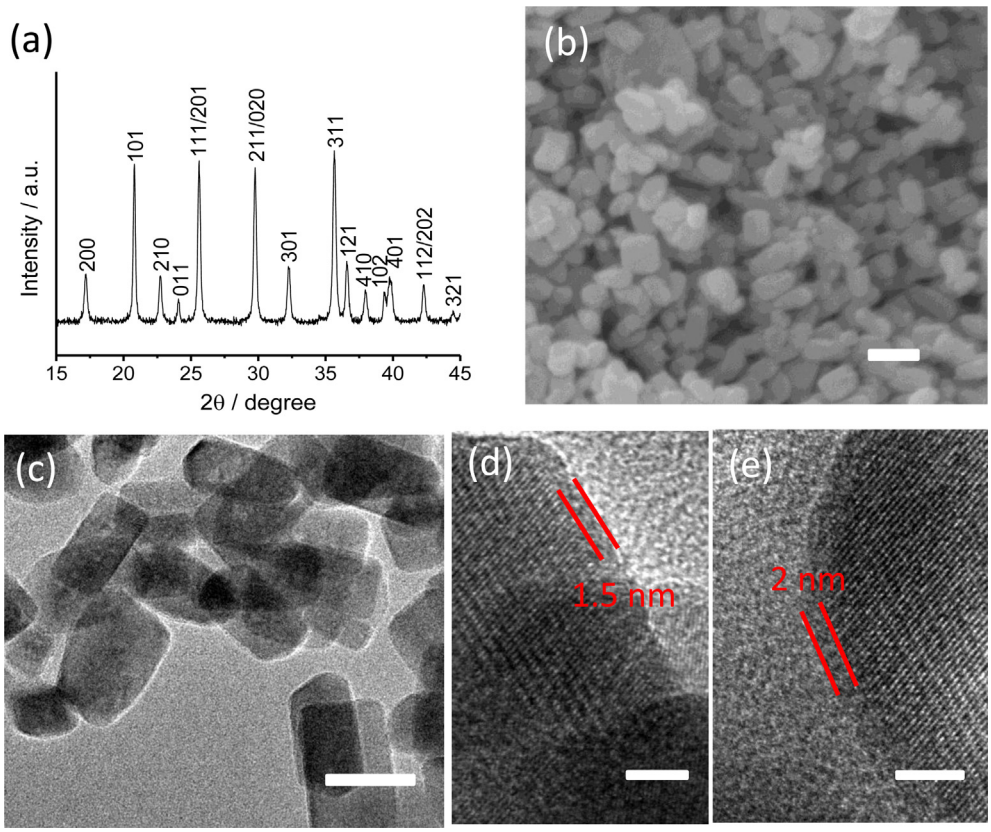

Fig. 4. Characterizations of carbon-coated $LiFePO_4$ nanocrystals: (a) XRD pattern; (b) SEM image; (c) TEM image; (d) and (e) HRTEM images. The thickness of the uniformly coated carbon shell on $LiFePO_4$ nanocrystals was about 1–2 nm. Scale bars: (b) 100 nm; (c) 50 nm; (d) and (e) 5 nm.

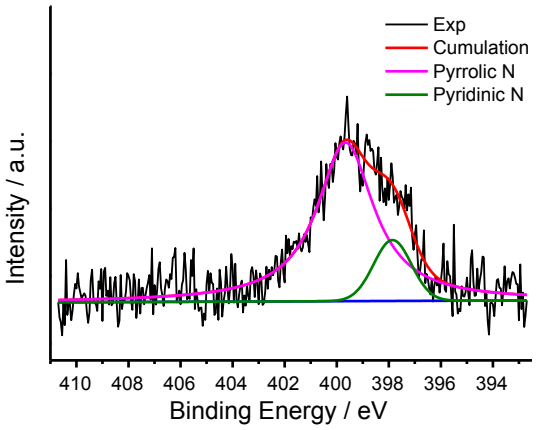

Fig. 5. N(1s) XPS spectrum of $LiFePO_4/C$, the peak located at 398 eV corresponds to pyridinic nitrogen, and peak located at 400 eV corresponds to pyrrolic nitrogen.

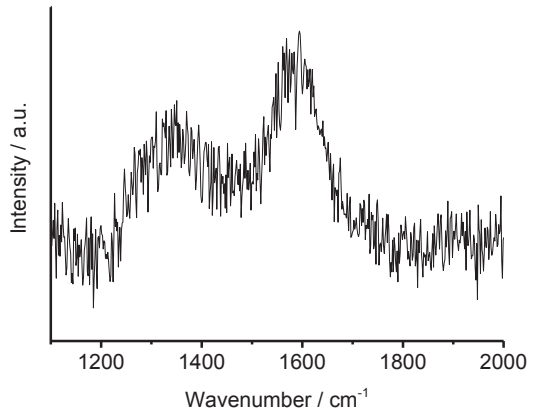

Fig. 6. Raman spectrum of $LiFePO_4/C$.

$LiFePO_4/C$ composite was then evaluated for its rate performance and cycle stability. Fig. 10a shows that discharge capacities of the $LiFePO_4/C$ composite at different C rates. A high capacity of 165 mAh g^{-1}, or 96.5% of the theoretical capacity of LFP, was obtained at 0.5 C. Even at a high discharge rate of 10 C, a remarkable specific capacity of 143 mAh g^{-1} (or 84% of theoretical capacity) was still possible with very low polarization of the discharge curves, which is a clear indication of the high rate performance of the composite.

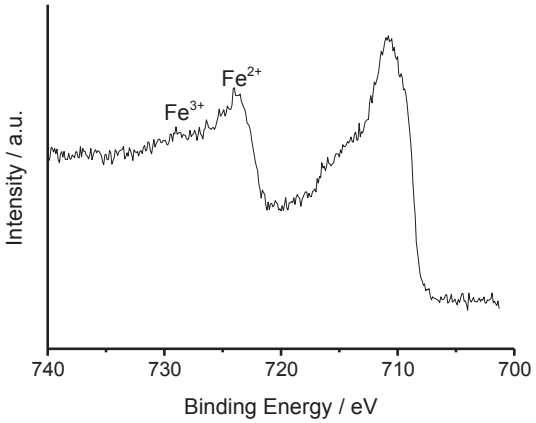

Fig. 7. Fe 2p spectrum of $LiFePO_4/C$.

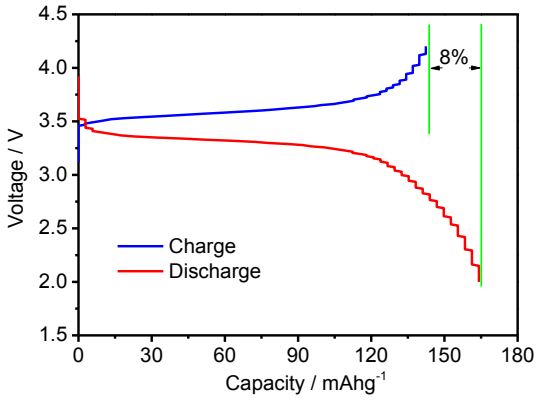

Fig. 8. First cycle charge and discharge profiles of $LiFePO_4/C$.

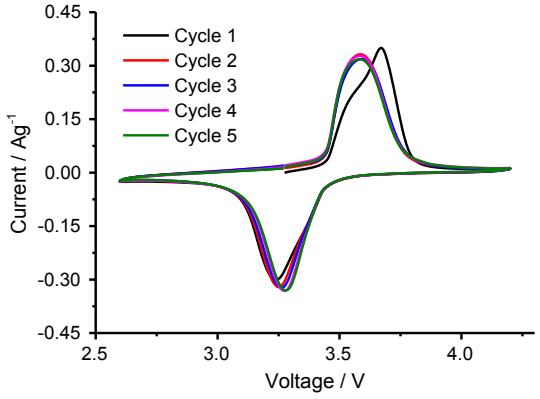

Fig. 9. Cyclic voltammograms of $LiFePO_4/C$ at 0.1 mV s^{-1}.

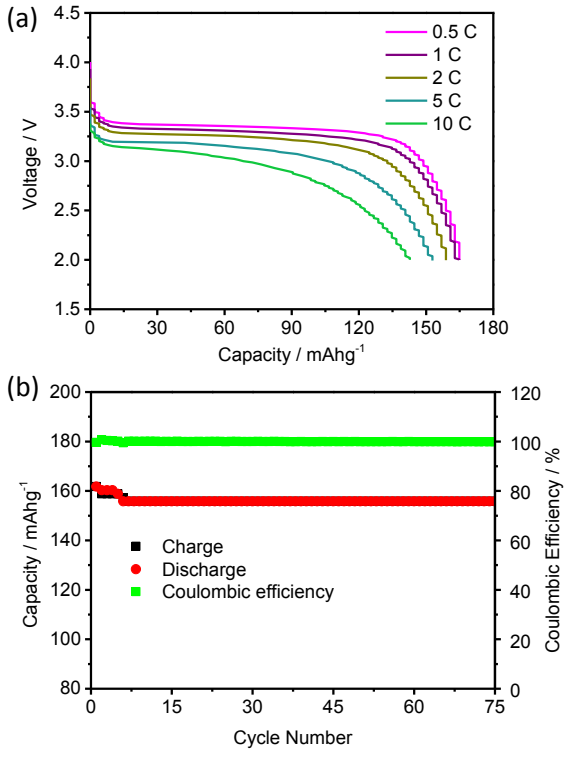

Fig. 10. Electrochemical performance of $LiFePO_4/C$: (a) rate capability; (b) cycle stability.

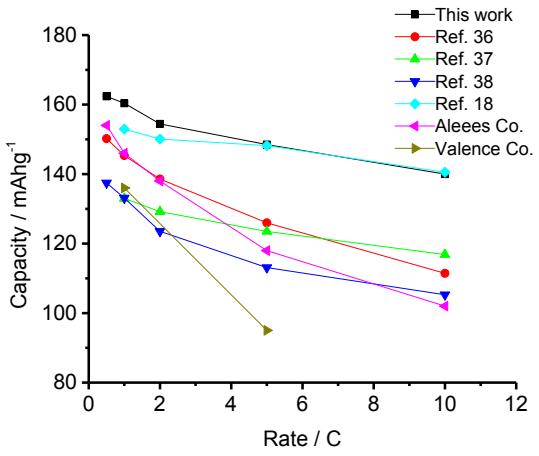

Fig. 11. Comparison of rate performance with recently published high rate $LiFePO_4$ and commercial $LiFePO_4$.

The cyclability of the $LiFePO_4$/C composite at 2 C is shown in Fig. 10b. Prior to the measurements the cells were conditioned by cycling at 0.5 C for 5 cycles. The composite displayed very good stability with no capacity loss, and columbic efficiencies greater than 99.8% for 75 cycles. The contributions of the uniform and fully encapsulating carbon coating on each nanocrystal to the reversibility of Li^+ intercalation/de-intercalation and consequently capacity retention were corroborated by these measurements. The capacity of the $LiFePO_4$/C composite as shown in Fig. 11 clearly demonstrates the exceptional power capability of the ultrathin carbon-coated $LiFePO_4$/C synthesized here. Given that the amount of carbon in the composite synthesized as such is extremely low, this synthesis method should be of strong interest to real applications.

4. Conclusions

In summary, an expeditious method of using dopamine as carbon precursor to impart good surface conductivity to $LiFePO_4$ nanocrystals is presented here. The *in-situ* polymerization of adsorbed dopamine to polydopamine only makes use of the indigenous Fe^{3+} ions on the $LiFePO_4$ surface without the need for extraneous chemicals. The self-limiting polymerization forms a thin and continuous deposit on the $LiFePO_4$ nanocrystals, which is then converted into a highly graphitized, N-doped carbon coating by high temperature calcination. The presence of the polydopamine coating is found to be effective in inhibiting crystal growth during calcination. The $LiFePO_4$/C composite synthesized as such is found to exhibit excellent rate capability and cycle stability. The exceptional electrochemical performance could be attributed to the contributions from the ultrathin and uniform carbon shell on nanocrystalline $LiFePO_4$ to the increase in electronic and ionic conductivities without mutually compensating effects.

Acknowledgements

This work was supported by the National University of Singapore Graduate School for Integrative Sciences and Engineering (NGS).

References

[1] A.K. Padhi, K.S. Nanjundaswamy, J.B. Goodenough, J. Electrochem. Soc. 144 (1997) 1188–1194.
[2] A. Yamada, S.C. Chung, K. Hinokuma, J. Electrochem. Soc. 148 (2001) A224–A229.
[3] S.-Y. Chung, J.T. Bloking, Y.-M. Chiang, Nat. Mater. 1 (2002) 123–128.
[4] A.S. Arico, P. Bruce, B. Scrosati, J.-M. Tarascon, W. van Schalkwijk, Nat. Mater. 4 (2005) 366–377.
[5] F. Yu, S.G. Chen, Y. Chen, H.M. Li, L. Yang, Y.Y. Chen, Y.S. Yin, J. Mol. Struct. 982 (2010) 152–161.
[6] G. Li, H. Azuma, M. Tohda, Electrochem. Solid-State Lett. 5 (2002) A135–A137.
[7] Y. Wang, P. He, H. Zhou, Energy Environ. Sci. 4 (2011) 805–817.
[8] D. Jugović, D. Uskoković, J. Power Sources 190 (2009) 538–544.
[9] L.-X. Yuan, Z.-H. Wang, W.-X. Zhang, X.-L. Hu, J.-T. Chen, Y.-H. Huang, J.B. Goodenough, Energy Environ. Sci. 4 (2011) 269–284.
[10] J. Wang, X. Sun, Energy Environ. Sci. 5 (2012) 5163–5185.
[11] H.M. Xie, R.S. Wang, J.R. Ying, L.Y. Zhang, A.F. Jalbout, H.Y. Yu, G.L. Yang, X.M. Pan, Z.M. Su, Adv. Mater. 18 (2006) 2609–2613.
[12] Y.-H. Huang, J.B. Goodenough, Chem. Mater. 20 (2008) 7237–7241.
[13] Y.S. Hu, Y.G. Guo, R. Dominko, M. Gaberscek, J. Jamnik, J. Maier, Adv. Mater. 19 (2007) 1963–1966.
[14] X.-L. Wu, L.-Y. Jiang, F.-F. Cao, Y.-G. Guo, L.-J. Wan, Adv. Mater. 21 (2009) 2710–2714.
[15] Y. Yin, M. Gao, H. Pan, L. Shen, X. Ye, Y. Liu, P.S. Fedkiw, X. Zhang, J. Power Sources 199 (2012) 256–262.
[16] Y. Lin, M. Gao, D. Zhu, Y. Liu, H. Pan, J. Power Sources 184 (2008) 444–448.
[17] Y. Wang, Y. Wang, E. Hosono, K. Wang, H. Zhou, Angew. Chem. Int. Ed. 47 (2008) 7461–7465.
[18] L. Wang, X. He, W. Sun, J. Wang, Y. Li, S. Fan, Nano Lett. 12 (2012) 5632–5636.
[19] K. Saravanan, M.V. Reddy, P. Balaya, H. Gong, B.V.R. Chowdari, J.J. Vittal, J. Mater. Chem. 19 (2009) 605–610.
[20] K. Saravanan, P. Balaya, M.V. Reddy, B.V.R. Chowdari, J.J. Vittal, Energy Environ. Sci. 3 (2010) 457–463.
[21] C. Nan, J. Lu, C. Chen, Q. Peng, Y. Li, J. Mater. Chem. 21 (2011) 9994–9996.
[22] S.-P. Badi, M. Wagemaker, B.L. Ellis, D.P. Singh, W.J.H. Borghols, W.H. Kan, D.H. Ryan, F.M. Mulder, L.F. Nazar, J. Mater. Chem. 21 (2011) 10085–10093.
[23] G. Kobayashi, S.-i. Nishimura, M.-S. Park, R. Kanno, M. Yashima, T. Ida, A. Yamada, Adv. Funct. Mater. 19 (2009) 395–403.
[24] J.F. Martin, A. Yamada, G. Kobayashi, S.-i. Nishimura, R. Kanno, D. Guyomard, N. Dupré, Electrochem. Solid-State Lett. 11 (2008) A12–A16.
[25] Q. Wei, F. Zhang, J. Li, B. Li, C. Zhao, Polym. Chem. 1 (2010) 1430–1433.
[26] J. Cui, Y. Wang, A. Postma, J. Hao, L. Hosta-Rigau, F. Caruso, Adv. Funct. Mater. 20 (2010) 1625–1631.
[27] A. Postma, Y. Yan, Y. Wang, A.N. Zelikin, E. Tjipto, F. Caruso, Chem. Mater. 21 (2009) 3042–3044.
[28] H. Lee, S.M. Dellatore, W.M. Miller, P.B. Messersmith, Science 318 (2007) 426–430.
[29] F. Bernsmann, B. Frisch, C. Ringwald, V. Ball, J. Colloid Interface Sci. 344 (2010) 54–60.
[30] S. Hong, Y.S. Na, S. Choi, I.T. Song, W.Y. Kim, H. Lee, Adv. Funct. Mater. 22 (2012) 4711–4717.
[31] C. Lei, F. Han, D. Li, W.-C. Li, Q. Sun, X.-Q. Zhang, A.-H. Lu, Nanoscale 5 (2013) 1168–1175.
[32] J. Kong, W.A. Yee, L. Yang, Y. Wei, S.L. Phua, H.G. Ong, J.M. Ang, X. Li, X. Lu, Chem. Commun. 48 (2012) 10316–10318.
[33] A.J. Bard, L.R. Faulkner, Electrochemical Methods: Fundamentals and Applications, Wiley, New York, 1980.
[34] J.P. Paraknowitsch, J. Zhang, D. Su, A. Thomas, M. Antonietti, Adv. Mater. 22 (2010) 87–92.
[35] W. Yang, T.-P. Fellinger, M. Antonietti, J. Am. Chem. Soc. 133 (2010) 206–209.
[36] S.W. Oh, S.-T. Myung, S.-M. Oh, K.H. Oh, K. Amine, B. Scrosati, Y.-K. Sun, Adv. Mater. 22 (2010) 4842–4845.
[37] G. Wang, H. Liu, J. Liu, S. Qiao, G.M. Lu, P. Munroe, H. Ahn, Adv. Mater. 22 (2010) 4944–4948.
[38] X. Zhou, F. Wang, Y. Zhu, Z. Liu, J. Mater. Chem. 21 (2011) 3353–3358.
[39] U. Chandra, B.E. Kumara Swamy, O. Gilbert, B.S. Sherigara, Electrochim. Acta 55 (2010) 7166–7174.
[40] P.H. Yan, J.Q. Wang, L. Wang, B. Liu, Z.Q. Lei, S.R. Yang, Appl. Surf. Sci. 257 (2011) 4849–4855.
[41] B.C. Zhu, S. Edmondson, Polymer 52 (2011) 2141–2149.
[42] N. Ravet, M. Gauthier, K. Zaghib, J.B. Goodenough, A. Mauger, F. Gendron, Julien, Chem. Mater. 19 (2007) 2595–2602.
[43] X.-F. Guo, H. Zhan, Y.-H. Zhou, Solid State Ionics 180 (2009) 386–391.
[44] Y. Wang, J. Wang, J. Yang, Y. Nuli, Adv. Funct. Mater. 16 (2006) 2135–2140.